Temporal scaling in *C. elegans* larval development

Olga Filina[1], Rik Haagmans[1] and Jeroen S. van Zon[1*]

[1]AMOLF, Science Park 104, 1098 XG Amsterdam, the Netherlands.

[*]Corresponding author: j.v.zon@amolf.nl

Abstract

It is essential that correct temporal order of cellular events is maintained during animal development. During post-embryonic development, the duration of development depends on external conditions, such as food availability, diet and temperature. How timing of cellular events is impacted when the rate of development is changed is not known. We used a novel time-lapse microscopy approach to simultaneously measure the timing of oscillatory gene expression, seam cell divisions and cuticle shedding in individual animals during *C. elegans* larval development. We then studied how timing of these events was impacted by changes in temperature or diet, and in *lin-42/Period* mutants that show strongly perturbed and heterogeneous timing of larval development. We uncovered significant variability in timing between individuals under the same conditions. However, we found that changes in timing between individuals were fully explained by temporal scaling, meaning that each event occurred at the same relative time, when rescaled by the total duration of development in each individual. Upon changing conditions, we found that larval development separated into distinct epochs that differed in developmental rate. Changes in timing of individual events were fully captured by temporal scaling for events occurring within each epoch, but not for events from different epochs. Overall, our results reveal a surprisingly simple structure that governs changes in timing of development in response to environmental conditions. The unexpected observation of continued development and accurate temporal scaling in growth-arrested *lin-42* mutants rules out a mechanism that explains temporal scaling by linking developmental timing to body size.

Introduction

Numerous cellular events that occur during animal development, such as cell division, cell movement and gene expression, must be tightly coordinated in time to allow formation of a functional organism with a correctly established body plan. However, despite our increasing understanding of the regulation of developmental timing[1-3], how cells in developing organisms measure time and execute events in the correct temporal order remains poorly understood. Moreover, the rate of post-embryonic development in animals is significantly affected by external conditions, such as food availability, diet and temperature. For example, severe dietary restriction extends the duration of larval development in the nematode worm *C. elegans* as much as ten-fold, without resulting in apparent defects in development[4]. How the timing of individual developmental events is adjusted in response to such changes in the organism-level rate of development is not known.

This question about developmental timing has a parallel in the context of spatial patterning during development. It has been shown that spatial gene expression patterns often scale with organ or embryo size, i.e. with the spatial pattern adjusted in each individual organ or embryo so that the spatial features occurred at the same position relative to its overall size[5-8]. For example, in *Drosophila* embryos gap genes are expressed in bands along the anteroposterior body axis[9, 10]. These bands have highly stereotypical positions relative to the embryo's size, even though this size shows significant variability between individuals[6]. Moreover, embryos of closely related species that vary greatly in size exhibit the same number of bands with similar position relative to the size of the embryo[6]. Here, we examine the possibility that, analogous to scaling of spatial patterns in development, the timing of development exhibits temporal scaling, meaning that, when the organism-level rate of development is changed, the timing of individual events is adjusted so that they still occur at the same time, when measured relative to the total duration of development. Such a mechanism would ensure the correct synchrony of developmental events even when organism-level timing is changed in an unpredictable manner by shifts in external conditions.

Due to its invariant cell lineage and highly stereotypical development. *C. elegans* is an ideal model organism to study developmental timing. Its postembryonic development consists of four larval stages (L1-L4) that are separated by a molting event, where a new cuticle is synthesized and the old cuticle shed[11]. After the final L4 molt, animals reach reproductive maturity, marking their transition into adulthood. There is a clear periodic aspect to *C. elegans* development, with molts occurring every 8-10 hours at 25˚C. Moreover, larval stages are

accompanied by genome-wide oscillatory expression of a multitude of genes, with peaks occurring once per larval stage[12-14].

Developmental timing has been extensively studied in *C. elegans*, leading to the discovery of heterochronic genes[2, 3]. Most heterochronic mutants impact timing in a specific larval stage, with events in that larval stage shifted to an earlier stage or repeated in subsequent stages[15], but do not appear to strongly perturb developmental timing on the organism level. An exception is the heterochronic gene *lin-42*, which is expressed in an oscillatory manner during development, peaking once every larval stage. In *lin-42* mutants, developmental timing is severely perturbed, with strong animal-to-animal variability in larval stage duration[16]. The body-wide, oscillatory expression dynamics of *lin-42,* together with its impact on larval stage duration, makes *lin-42* an interesting candidate for a global regulator of developmental timing. Intriguingly, *lin-42* is a homolog of Period, an important component of the circadian clock in *Drosophila* and higher organisms[17]. Hence, it has been speculated that *lin-42* may form part of a time-keeping mechanism that allows cells and organs to read out developmental time[11].

How timing of individual events is impacted by changes in the organism-level rate of development is poorly characterized. Timing of *C. elegans* larval development is often measured at the population level, by examining the developmental stage of animals sampled from age-synchronized populations. This approach has limited time resolution and does not allow measuring timing of multiple events within the same individual. This is a particular problem for mutants such as *lin-42*, where developmental synchrony between individual animals is lost. However, the alternative approach of following individual animals was so far performed manually, limiting the number of animals that could be examined. We have recently developed a novel microscopy approach that allows automated imaging of individual *C. elegans* larvae during their entire development and at single-cell resolution[18], making it possible to measure timing of cellular events in many individual larvae.

Here, we used this approach to simultaneously measure the timing of three different developmental events (oscillatory expression of a molting cycle gene, seam cell divisions and cuticle shedding) in individual *C. elegans* larvae, both under changes in environmental conditions (temperature and diet) and in mutant animals, where the duration of larval development was increased up to ~3-fold. We indeed observed temporal scaling of the timing of these events. First, for isogenic populations under the same environmental conditions, we observed strong variability in timing between animals, yet all events occurred at similar times when measured relative to the total duration of development for each individual. This

observation implied that animals progressed through development at a constant developmental rate, with variability in timing dominated by differences in this rate between individuals.

Second, when we changed the duration of development on the population level, e.g. by changing environmental conditions or in mutants, development was split into distinct epochs that differed in how timing was impacted, with the number and duration of epochs depending on the exact condition. While timing of events did not always scale with total duration of development, when comparing between populations that different in duration of development, events did occur at the same time relative to the duration of the epoch they occurred in. Surprisingly, temporal scaling, both with inter-individual variability in timing and population-averaged changes in duration of epochs, was observed for *lin-42(0)* mutants, that showed strongly delayed and highly heterogeneous timing of larval development, and even in *lin-42(0)* individuals that fully arrested physical growth mid-development.

Overall, these results are the first to demonstrate precise scaling of the timing of cellular events during *C. elegans* post-embryonic development, thereby revealing precise adaptation of cell-level timing to changes in the organism-level rate of development under a wide range of conditions. Moreover, the observation of temporal scaling in growth-arrested *lin-42(0)* individuals rules out a model that explains temporal scaling by initiating each event at a specific body size. Hence, our observations raise the important question how temporal scaling is incorporated by the as-yet unknown molecular mechanisms that control developmental timing.

Results

To examine how developmental timing is coordinated ion the organism-level in developing *C. elegans* larvae, we measured the timing of multiple developmental events that occurred frequently and throughout all of larval development. In particular, we quantified timing of seam cell divisions, oscillatory gene expression and ecdysis. Seam cells are hypodermal stem cell-like cells that divide asymmetrically once every larval stage, giving rise to one hypodermal cell and one seam cell (Fig. 1a,d)[19]. In addition, several seam cells (V1-V4 and V6) undergo a symmetric division in the L2 larval stage, doubling their number. Oscillatory gene expression is a pervasive phenomenon in *C. elegans*, with thousands of gene transcripts oscillating during development with a periodicity corresponding to that of the molting cycle[12-14]. Here, we focused on the oscillatory gene *wrt-2*, a hedgehog-like protein expressed in the seam cells, that peaks in expression once every larval stage[12, 18] (Fig. 1b,d). Finally, ecdysis is the shedding of the old cuticle at the end of each larval stage (Fig. 1c,d). By focusing on these three events, we captured qualitatively different developmental processes, while their repetitive nature allowed us to capture many events in a single experiment (Fig. 1d).

To accurately measure the timing of individual events, we used a novel fluorescence time-lapse microscopy approach to follow the full ~40 h of post-embryonic development of individual *C. elegans* larvae with single-cell resolution[18]. Briefly, embryos were placed inside hydrogel chambers filled with *E. coli* as a food source. These chambers contained sufficient food to sustain development into adulthood, while constraining animals to the field of view of the microscope at each stage. By capturing fluorescence and transmitted light images with fast, 1-10 ms, exposure time, we could image developmental dynamics with single-cell resolution in moving larvae, without the need for immobilizing animals.

To visualize seam cell division, we used the strain *heIs63[wrt-2p::H2B::GFP, wrt-2p::PH::GFP]*, where green fluorescent protein (GFP) was targeted specifically to the nucleus and the membrane of the seam cells[20]. Since divisions of individual seam cells occurred close together in time, we defined the time of each round of divisions as the average time at which V1-V6 cells have divided or started dividing, as determined by the formation of the metaphase plate. Because the reporter used to detect seam cell divisions (*heIs63*) produces GFP under control of the *wrt-2* promoter, it enabled simultaneous measurement of oscillatory *wrt-2* expression. Fluorescent images were analyzed automatically using custom-written software to extract the mean fluorescent intensity of the *wrt-2* reporter in seam cell nuclei at every time frame. Finally, the time of expression peaks was extracted from the resulting oscillatory *wrt-2* expression

profiles, by fitting their dynamics with a combination of Gaussian functions and a linear offset (Fig. 1b, Eq. 1 in Methods). Finally, the time of the ecdysis was defined as the time when the shed cuticle first became visible in the transmitted light image (Fig. 1c). Full details on data acquisition and analysis are provided in the Methods section.

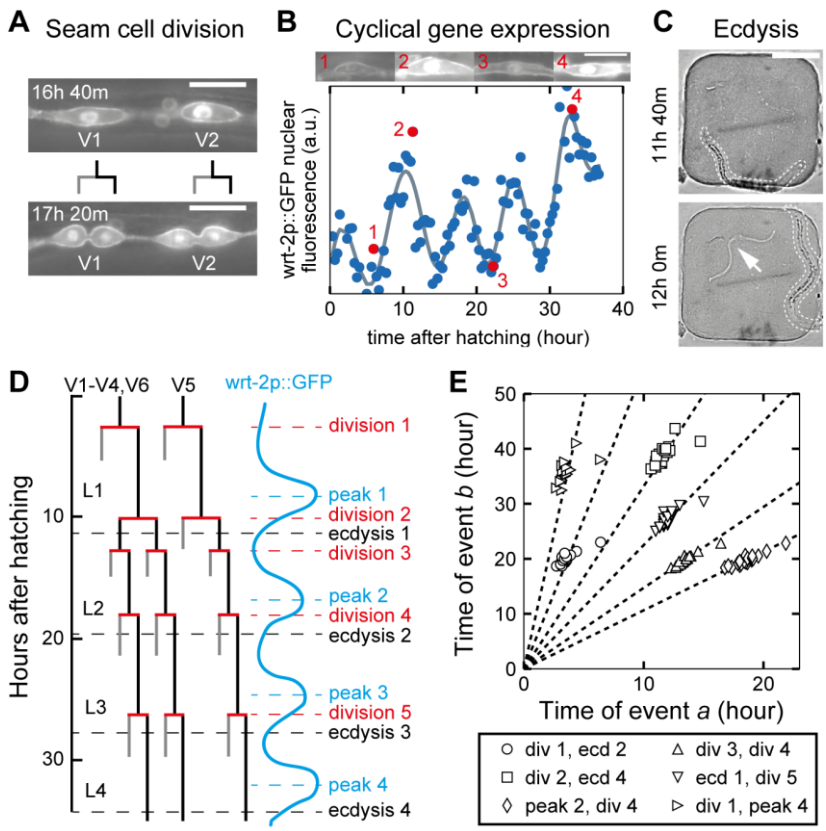

Figure 1. **Scaling of developmental timing in individual animals**

(a)-(c) Measuring timing of seam cell division, cyclical gene expression and ecdysis. **(a)** Seam cells divide once or twice every larval stage giving rise either to hypodermal (grey line) or seam cell (black line) daughters. We determined the timing of the V1-V6 seam cells by directly observing seam cell division in the *wrt-2p::GFP::PH; wrt-2p::GFP::H2B* fluorescent reporter (*wrt-2p::GFP*). Scale bar: 15 μm. **(b)** Expression of *wrt-2* peaks once every larval stage and was visualized in seam cells in *wrt-2p::GFP* animals (top panel, posterior V3 seam cell). We quantified *wrt-2p::GFP* fluorescence averaged over the V1-V6 seam cells (lower panel) and fitted the data to Eq. 1 (grey line) to determine the time of each expression peak. Red markers correspond to the time points shown in the top panel. Scale bar: 15 μm. **(c)** The time of ecdysis was determined by the appearance of a shed cuticle (arrow) away from the larva (outlined).

Scale bar: 100 μm. **(d)** Schematic overview of seam cell division, *wrt-2* peak and ecdysis events during post-embryonic development. **(e)** Measured times of event pairs a, b in wild-type animals, on an *E. coli* OP50 diet at 23˚C, with each marker indicating event times measured in a single animal (n=21). Times of event pairs show temporal scaling, i.e. they lie clustered along lines of constant $\frac{t_b}{t_a}$, even as individual event times t_a and t_b show significant variability. Dashed lines are fits of the form t_b=$s_{a,b} \cdot t_a$.

Scaling of developmental timing in individual animals

We first quantified timing of seam cell division, *wrt-2* expression peaks and ecdysis in wild-type animal in the standard condition, on a diet of *E. coli* OP50 at 23°C (Fig. 1e). We found that individual animals showed variability in the total duration of development, with a ~10 h difference observed between the first and last animal to enter adulthood, as measured by completion of the L4 ecdysis (~40 h after hatching). Such animal-level variability in timing has been observed before and was linked to the age of the mother when the egg was fertilized[18, 21]. We also observed variability in the timing of individual developmental events. Interestingly, this variability was strongly correlated: when we plotted event times t_a and t_b against each other, for different pairs of events a, b, all data points clustered along a line (Fig. 1e). This strong correlation was even present for pairs of events that are separated in time by ~30 h, such as the L1 seam cell division and the L4 *wrt-2* peak.

A simple argument explains this observation as a manifestation of temporal scaling: if the time t_a of each event a scales with the total duration of development T, then the fraction t_a/T has a constant value C_a, even when t_a and T vary significantly between individuals. Then, the time at which two events a and b occur in same individual is related by $t_b = \frac{C_b}{C_a} t_a$, independent of total duration of development T in that individual. As a result, measurements for individual animals will be clustered along a line of constant $\frac{t_b}{t_a}$, as observed experimentally. Strikingly, this observation holds for all pairs of events we examined (Supplementary Fig. 1), meaning that if an animal executed its first seam cell division earlier than the rest of the population, it was highly likely to be similarly early in executing all subsequent events for the rest of larval development. Indeed, we could fully capture these experimental results with a simple stochastic timing model (Fig. 2a, Supplementary Fig. 2, Eq. 2 and 3), if we assumed that the observed variability in timing was dominated by animal-to-animal variation in the organism-level rate of development,

$1/T$, that otherwise remained constant throughout development. Overall, our results show that the measured changes in timing between individuals can be fully explained by simple rescaling with the total duration of development in each individual.

Scaling of developmental timing upon changes in temperature

Changes in environmental conditions typically increase or decrease the population-averaged duration of development, yet how timing of cell-level events is adjusted to such changes in organism-level timing is an open question. To address this question, we first measured event timing in individual animals maintained at different temperatures, as the duration of larval development increases with decreasing temperatures[22]. As expected, we observed that as temperature was reduced from the standard temperature of 23˚C to 19˚C and 15˚C, the duration of post-embryonic development increased from 39±2 to 57±1 and 105±2 hours, respectively (Supplementary Fig. 3). Likewise, we found that individual events were delayed more strongly with decreasing temperature (Fig. 2a).

To examine the impact of changing temperatures on average event timing, we defined, as measure of developmental progression, the phase $\phi_a = \langle t_a^S \rangle / \langle T^S \rangle$, where $\langle t_a^S \rangle$ and $\langle T^S \rangle$ are the average time of event a and the duration of development measured under standard conditions (23˚C), and ϕ=0 and 1 correspond to the start of larval development and adulthood. This definition ensures that under standard conditions the developmental phase ϕ increases with constant rate $1/\langle T^S \rangle$ (Fig. 2b). If the total duration of development increases or decreases, e.g. due to shifting environmental conditions, $\phi(t)$ will change, so that the same developmental phase ϕ is reached at a different time t compared to standard conditions. Indeed, when we measured the average time of each seam cell division, wrt-2p::GFP peak and ecdysis for 19˚C and 15˚C, we found that the phase still increased linearly with time, but at a lower rate compared to 23˚C (Fig. 2b).

When we examined events times in individuals, we found similar variability in timing for animals at 19˚C and 15˚C compared to 23˚C. Moreover, times of event pairs still clustered along lines, meaning that temporal scaling with inter-individual variability in the duration of development occurred also for these conditions (Fig. 2c). Strikingly, event pairs clustered along the exact same line independent of temperature. This is a manifestation of population-level temporal scaling, i.e. for all three temperatures events occurred at the same relative time, when

rescaled with the population-averaged duration of development observed for each temperature, even as development at 15˚C was slowed ~3-fold compared to 23˚C.

To test whether temporal scaling with the population-level change in developmental duration explained timing for all measured event pairs, we used the following approach. First, we calculated for each event pair a and b measured in an individual animal, the angle $\theta = \arctan \frac{t_a}{t_b}$ (See Methods for details). Then, we calculated $\delta = \langle \theta^P \rangle - \langle \theta^S \rangle$, the difference between the average angle for standard (S, 23˚C) and perturbed (P, 19˚C or 15˚C) conditions, with $\delta \approx 0$ indicating that the data for standard and perturbed conditions clustered along the same line. In addition, we also used the two-sample Kolmogorov-Smirnov test to estimate the probability that the θ distributions measured for standard and perturbed conditions were draw from the same distribution. This analysis showed that most event pairs at 15˚C and 19˚C (Fig. 2d,e) lie along the same line as data for 23˚C, i.e. changes in timing between temperatures are fully captured by temporal scaling with duration of development.

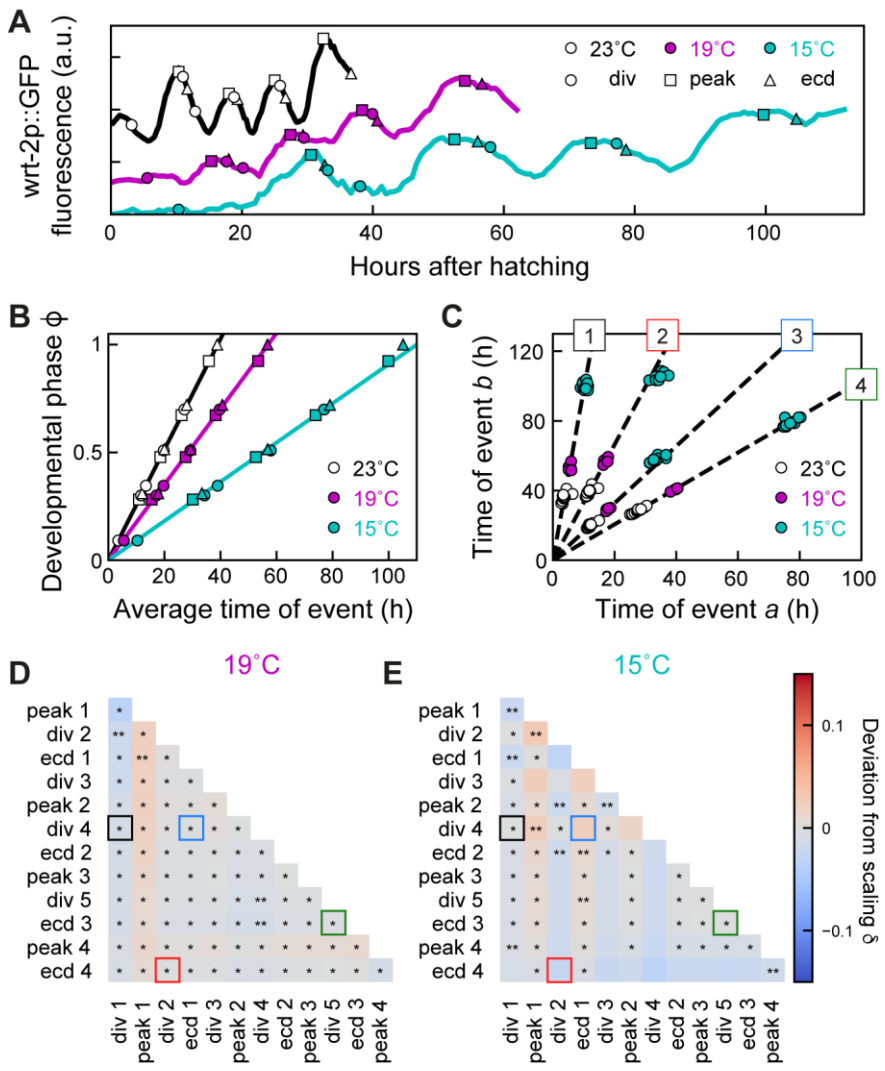

Figure 2. **Temporal scaling in developmental timing at different temperatures.**

(a) Examples of developmental timing in individual animals at standard conditions (23˚C, black), 19˚C (magenta) and 15˚C (cyan). Markers indicate the timing of seam cell divisions (circles), wrt-2p::GFP fluorescence peaks (squares) and ecdyses (triangles). Tracks are shifted along the vertical axis for clarity. **(b)** Developmental phase as function of time for different temperatures. Developmental progression is modeled as the evolution of a developmental phase ϕ in time. Each developmental event a occurs at a specific phase $\phi_a = \langle t_a^S \rangle / \langle T^S \rangle$, where $\langle t_a^S \rangle$ and $\langle T^S \rangle$ are the population-averaged time of event a and total duration of development for standard conditions. With this definition, the phase for standard conditions (black line) increases linearly with rate $1/\langle T^S \rangle$. Markers indicate the events as in (a). For 19˚C or 15˚C, the dependence of

phase on the average measured event times is well fitted by the 'Uniform' model, defined in Fig. 3 (magenta and cyan line). **(c)** Measured times for different event pairs: (1) division 1 and 4, (2) division 2 and ecdysis 4, (3) ecdysis 1 and division 4, and (4) division 5 and ecdysis 3. Lines are a linear fit to data for standard conditions (23˚C). For each event pair, most points for different temperatures cluster along the same line, indicating that changes in timing were explained by temporal scaling. **(d),(e)** Deviation from scaling for all event pairs for development at (d) 19˚C and (e) 15˚C. In addition, stars indicate the probability that data for standard conditions and 19˚C or 15˚C observe the same scaling relation, as assessed by a Kolmogorov-Smirnov (K-S) test, *:N.S., **:P<0.01, and P<0.001 otherwise. For animals at 19˚C, temporal scaling was observed for all event pairs, while some significant deviations were seen at 15˚C. Outlined squares correspond to event pairs in (c).

We could reproduce these observations with a simple, phenomenological model ('Uniform' model, Fig. 3). We assumed that population-averaged changes in timing resulted from a uniformly lowered rate of development, as observed experimentally (Fig. 2b, 3a), and included both an animal-to-animal variation in this rate, that remained constant throughout development, as well as variability in the phase of each individual event (Eq. 3). Stochastic simulations showed that when variability was dominated by the variation in developmental rate, the times of event pairs were positioned along a line (Fig. 3b-d). Moreover, this line was the same as for the corresponding events under standard conditions, with model calculations showing that the deviation $\delta=0$ for all event pairs (Eq. 6).

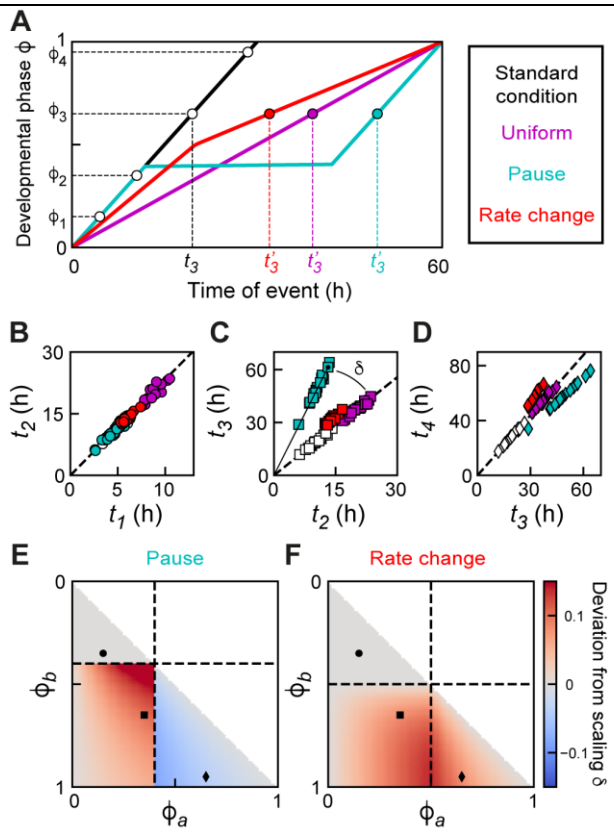

Figure 3. **Timing models.**

(a) Developmental phase as function of time for three different models that generate the same increase in duration of development, either by a uniform lower rate of development (magenta), a single, discrete pause at ϕ' (cyan) or a non-uniform change in the rate of development at ϕ'' (red). **(b)-(d)** Simulated event times for the different event pairs indicated in (a) (See Methods for details). Marker color corresponds to the timing models in (a). For all models, times of event pairs are clustered along a line, i.e. occur at the same time when rescaled by each individuals duration of development. For the 'Uniform' model, times of event pairs lie along the scaling line for standard conditions (dashed line), meaning that they occur at the same time when rescaled by the population-averaged duration of development. However, the other models often deviate from this scaling line. The deviation from scaling δ is defined as the signed angle between these two lines, as indicated in (c). **(e)-(f)** Calculated deviation δ from scaling for different events pairs a and b for the 'Pause' (e) and 'Rate change' (f) model (Eqs. 7-9). Black markers correspond to the event pairs in (b)-(d) and the dashed lines to ϕ' (e) and ϕ'' (f). These results indicate that the timing models in (a) can be distinguished by measuring the deviation from population-level scaling under conditions and in mutants that increase the total duration of development.

Breakdown of population-level scaling upon changes in diet

To test whether temporal scaling is also observed under qualitatively different changes in environmental conditions, we studied the impact of changes in food uptake and diet on timing of individual events. Total duration of development can be changed by providing animals with other food than *E. coli* OP50[23-25]. Here, we used two different approaches. To mimic reduced food uptake, we fed the standard diet, E. coli OP50, to *eat-2(ad1113)* mutants that exhibit a 5-fold decrease in pharyngeal pumping and hence ingest bacteria at lower rate[26]. In addition, we grew wild-type animals on a diet of E. coli HB101, which was reported to have faster larval development[23].

The total duration of development was slightly different in *eat-2* mutants (40±2h) and wild-type animals on HB101 (38±1h), compared to standard conditions of wild-type animals on OP50 (39±2h, Fig. 4a, Supplementary Fig. 3). However, we observed more complex changes in timing when we examined the average timing of seam cell divisions, *wrt-2* peaks and ecdyses (Fig. 4b). For *eat-2* mutants, the developmental phase increased linearly with time, albeit at a lower rate compared to standard conditions, as for the 'Uniform' model. However, for animals fed HB101 the increase of phase in time could not be fit by a single constant rate. Instead, the data from hatching to the third ecdysis was best fit with the phase increasing with the same rate as under standard conditions, but with a ~2h pause between the third seam cell division and second *wrt-2* peak during which the phase did not increase. For both non-standard diet conditions, we found that timing in individual animals showed significant variability, but times of event pairs were still clearly scattered along a line (Fig. 4c), indicating that event times scaled with inter-individual variability in developmental duration. However, while for *eat-1* mutants these data points were positioned along the same line as standard conditions, in animals fed HB101 we found that for some event pairs most points exhibited small, but systematic deviations from this line. This indicated that the differences in timing between animals fed OP50 and HB101 were not fully explained by rescaling with the population-averaged duration of development.

To understand the origin of these deviations, we constructed a phenomenological model analogous to the 'Uniform' model, but incorporating the pause inferred from the measured evolution of the developmental phase in time ('Pause' model, Fig. 3a, 4b). Inter-individual variability was taken into account as before, but with the variation impacting both the developmental rate and the duration of the pause. For the "Pause' model, the timing of event pairs still clustered along a line, but with slopes that differed from the equivalent lines for standard conditions (Fig. 3b-d), as observed experimentally. Interestingly, these deviations

occurred in a specific pattern (Fig. 3e): while timing of event pairs that both occurred before the developmental pause matched the line for standard conditions, deviations occurred when at least on event occurred after the pause. Event times clustered along a line with higher slope ($\delta > 0$) when one event occurred before and the other after the pause, with stronger deviations if both events were close to the pause. In contrast, when both events occurred after the pause, event times clustered along lines with lower slope ($\delta < 0$), with deviations stronger when events occurred farther apart in development.

We then tested these predictions from the 'Pause' model by calculating δ for all measured event pairs. As predicted, we found a clear difference between *eat-2* mutants on OP50 and wild-type animals on HB101 (Fig. 4d-e). Whereas data for *eat-2* mutants largely clustered along the lines predicted by data for standard conditions, the data for animals fed HB101 showed significant deviations. Interestingly, these deviations strongly resembled, both in magnitude and sign, those predicted by the 'Pause' model, with a positive deviation when one event occurs before and the other after the pause, and a negative deviation when both occur after.

Overall, these results show that changes in diet (HB101 instead of OP50) impact developmental timing in a manner that is more complex than rescaling with the population-averaged duration of development. However, the model suggests a simple picture that explains the experimental data: the lack of population-level temporal scaling results from the nonlinear increase of developmental phase in time seen for animals fed OP50, with a pause at the mid-L2 larval stage. Yet, each animal executes this temporal evolution of the developmental phase at an intrinsic speed that varies between individuals, still giving rise to inter-individual temporal scaling.

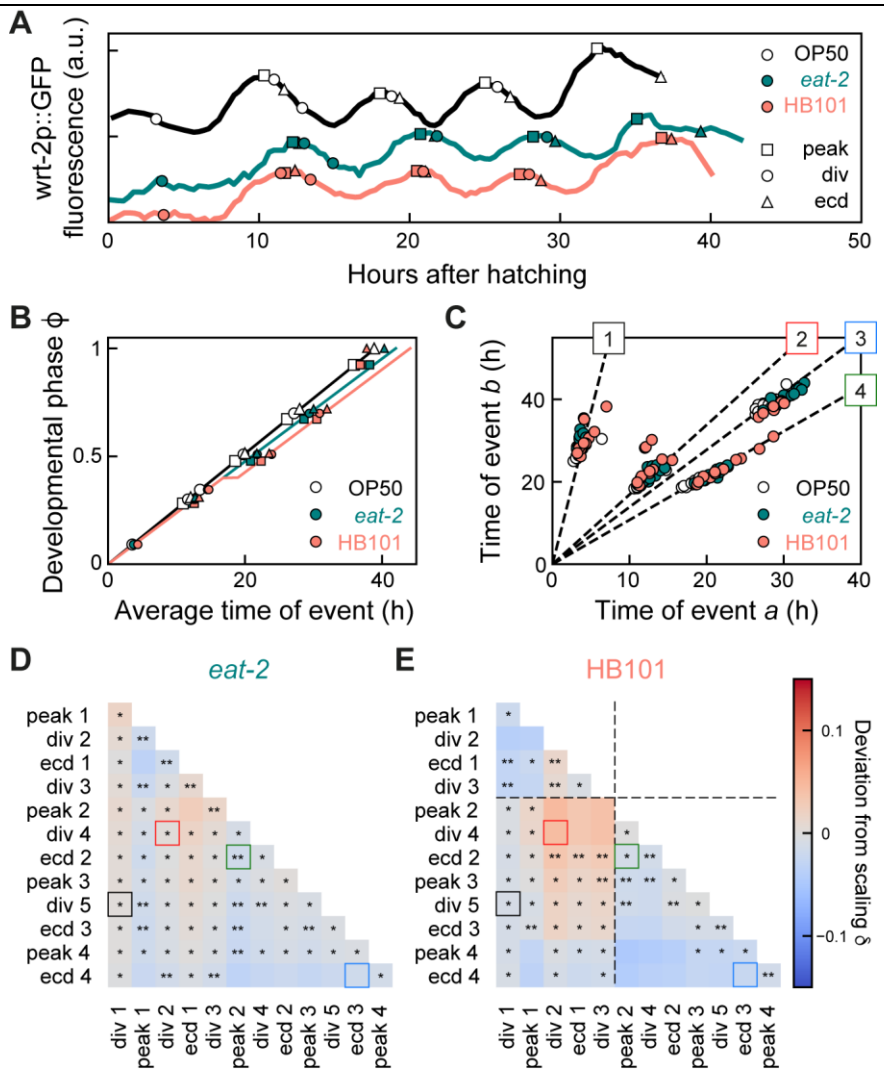

Figure 4. **Breakdown of temporal scaling for change in diet.**

(a) Developmental timing in individual animals in standard conditions (black: wild-type, *E. coli* OP50 diet) and two conditions that exhibit slow development: wild-type on *E. coli* HB101 (orange) and *eat-2* mutants, that have reduced food uptake, on *E. coli* OP50 (green). Markers indicate seam cell divisions (circles), wrt-2p::GFP peaks (squares) and ecdyses (triangles). **(b)** Developmental phase as function of time. Markers indicate events as in (a). For *eat-2* mutants, the phase evolution is well fitted by the 'Uniform' model (blue line), and for wild-type on HB101 by the 'Pause' model (orange line) with a pause of ~2h between seam cell division 3 and wrt-2p::GFP peak 2. **(c)** Measured times for event pairs: (1) division 1 and 5, (2) division 2 and 4, (3) peak 2 and ecdysis 2, and (4) ecdysis 3 and 4. Lines are a fit to data for standard conditions. For (2) and (3), animals on HB101 show systematic deviations from scaling. **(d),(e)** Deviation from scaling for development in (d) *eat-2* mutants and (e) on HB101. Stars indicate the probability that

the data observes the same scaling relation as on standard conditions: *:N.S., **:P<0.01, and P<0.001 otherwise (K-S test). Dashed lines in (e) indicate the time of the pause. While scaling is observed for almost all event pairs in *eat-2* mutants, animals on HB101 exhibit systematic deviations from scaling that resemble those predicted by the 'Pause' model.

Perturbed developmental timing and growth in *lin-42* mutants

For wild-type animals on HB101 we observed deviations from temporal scaling even as diet had only minor impact on total duration of development. To seek stronger perturbations of developmental timing and temporal scaling, we measured event timing in mutants of the heterochronic gene *lin-42*, for the following reasons. First, *lin-42* plays an important role in molting, with mutants showing longer larval stages, strongly reduced synchrony between individuals in progression through larval stages and frequent developmental arrest, with all these phenotypes increasing in severity as development proceeds[16, 27, 28]. Second, *lin-42* mutants exhibit heterochronic phenotypes in multiple organs[16, 17, 29, 30], indicating a body-wide role for *lin-42*. In addition, *lin-42* is expressed in many cells throughout the body and in a striking cyclical manner, with LIN-42 protein levels peaking once every larval stage[17]. This, together with the homology of *lin-42* to the circadian clock gene period, has led to the speculation that *lin-42* acts as a global developmental timer[11, 16]. Finally, *lin-42* regulates the expression of many miRNAs, including those involved in timing through the heterochronic pathway and binds to the promoter of many genes[31-33]. Because of this wide-ranging impact on developmental timing and gene expression, *lin-42* appeared a prime candidate for a core component of a potential scaling mechanism. Hence, we wanted to test whether *lin-42(0)* animals displayed a stronger breakdown of temporal scaling than observed under changes in diet.

We used the *lin-42(ox461)* allele that deletes the entire *lin-42* locus and shows the strongest perturbation of molting cycle progression[18]. Indeed, we found that postembryonic development at 23˚C was significantly slower in these *lin-42(0)* animals and showed much stronger variability both in the total duration of development (57±7h for *lin-42(0),* compared to 39±2h for wild-type animals) and the duration of individual larval stages (Supplementary Fig. 3). In addition, *lin-42(0)* animals showed reduced growth, as measured by the increase of body length over time in individual animals (Fig. 5a,b). In particular, we observed a fraction of animals that stopped growing completely between the L2 and L4 larval stage, with some reaching body lengths of only 0.3mm, compared to 0.9mm for wild-type animals. Surprisingly, all animals that arrested growth appeared to otherwise continue development: they underwent multiple rounds of

ecdysis, seam cell divisions and *wrt-2* expression peaks, albeit at much slower rate (Fig. 5c). Animals frequently skipped the final seam cell division and ecdysis, a heterochronic phenotype observed before [ref], but did so independently of the strength of the growth-arrest phenotype. After molting, *lin-42(0)* animals often remain stuck in their old cuticle, and it was suggested that this interferes with the ability to feed[27]. However, we observed growth arrest also in animals that appear to shed their cuticle normally. Moreover, growth-arrested animals also displayed pharyngeal pumping. These observations suggest that growth arrest was not simply caused by inability to take up food.

Breakdown of inter-individual and population-level temporal scaling in *lin-42* mutants

When we compared the average timing of each seam cell division, *wrt-2* peak and ecdysis between wild-type and *lin-42(0)* animals at 23˚C (Fig. 5d), we found that up until the L1 ecdysis and the third seam cell division, the developmental phase increased at the same rate in both cases. However, from the mid-L2 stage onward, starting with the second *wrt-2* peak, the phase still increased linearly in *lin-42(0)* mutants but with a strongly decreased rate compared to wild-type animals. When we examined timing in individual animals, we found that variability in timing was dramatically increased in *lin-42(0)* mutants. Yet, despite this strong variability data points for many event pairs still clustered along a line (Fig. 5e, Supplementary Fig. 4). However, this was not the case for all event pairs: for instance, some animals that were among the first to execute the third seam cell division exhibited an exceptionally late third *wrt-2* peak, resulting in many points away from the line (Fig. 5e, event pair 2). Hence, for this event pair, differences in timing between animals cannot be explained by inter-individual temporal scaling. Finally, for those event pairs that clustered along a line, data points often showed systematic deviations from the line predicted by data for standard conditions (wild-type animals at 23˚C) corresponding to a lack of population-level temporal scaling.

We then used the measured evolution of developmental phase to construct a phenomenological model of timing in *lin-42(0)* mutants ('Rate change' model, Fig. 3a, 5d). This model reproduced the experimental observation that data for most event pairs clustered along lines, but with systematic deviations from the lines predicted by data for standard conditions (Fig. 3b-d). In particular, for the 'Rate change' model these lines always had a larger slope than for standard conditions, i.e. $\delta \geq 0$ (Fig. 3f). Indeed, when we calculated δ for all experimentally measured event pairs (Fig. 5f) the resulting dependence of δ on the developmental phase

strongly resembled the prediction from the 'Rate change' model (Fig. 2f): first, the deviation was largest for event pairs with one event occurring prior to the mid-L2 larval stage, when we observed the change in developmental rate, and the other occurring afterwards. Second, in contrast to data for wild-type animals fed HB101, the deviation in *lin-42(0)* mutants was always positive ($\delta > 0$). These results suggested that the breakdown of population-level temporal scaling was largely accounted for by the decrease in developmental rate at the mid-L2 larval stage. Finally, compared to the rest of the population, growth-arrested animals did not develop more slowly, and their developmental timing did not exhibit stronger deviations from temporal scaling (Supplementary Fig. 4), suggesting that regulation of timing was not aversely affected by the lack of physical growth.

Overall, we uncovered significant deviations from temporal scaling in *lin-42(0)* animals. However, given the putative role of *lin-42* as a key regulator of developmental timing, it is interesting that loss of *lin-42* does not cause a general loss of accurate developmental timing, but for most events perturbs average timing and temporal scaling in a highly structured manner.

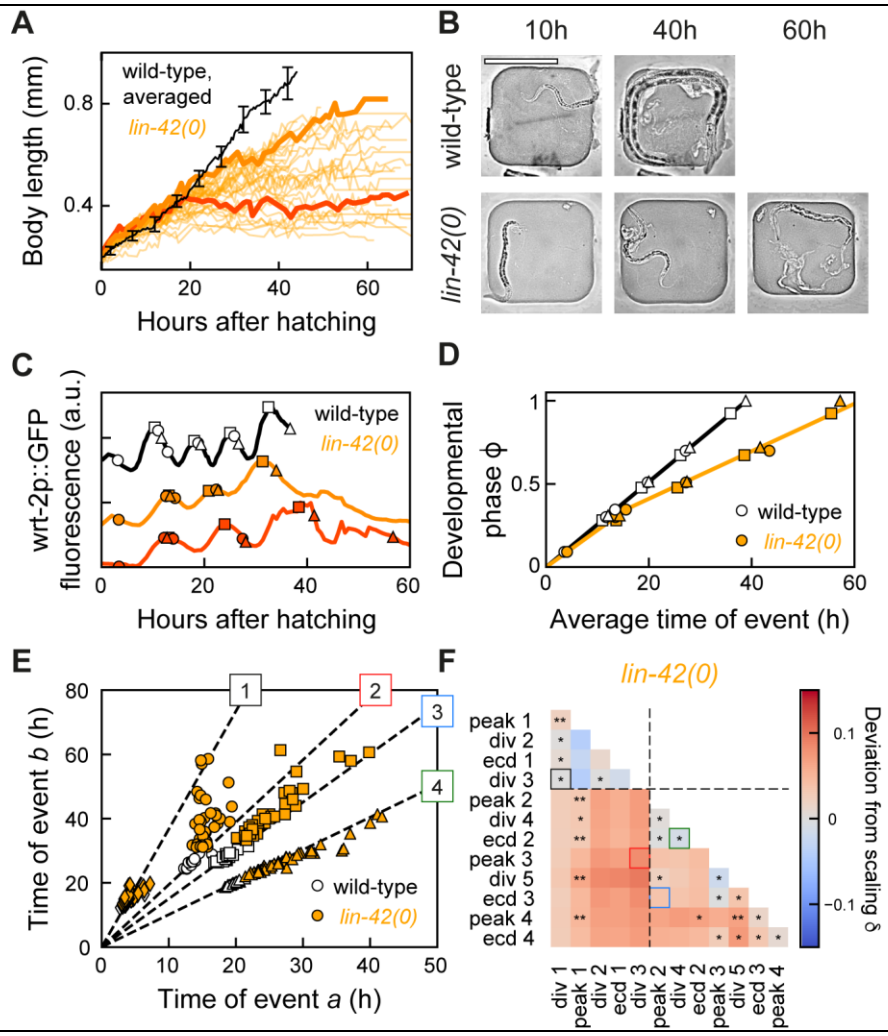

Figure 5. **Growth arrest and breakdown of temporal scaling in *lin-42(0)* animals.**

(a) Body length as a function of time after hatching for standard condition conditions (Average for wild-type animals at 23˚C, black) and *lin-42(0)* animals (orange). While some *lin-42(0)* animals exhibited reduced growth (light orange line), other animals showed a complete growth arrest from the mid-L2 stage, ~20 h after hatching, capping body length to <0.5mm (dark orange line). Error bars indicate S.E.M. **(b)** Microscopy images of a wild-type (upper panels) and growth-arrested *lin-42(0)* larva (lower panels) at different times after hatching. Scale bar is 200 µm. **(c)** Developmental timing in a wild-type larva (black) and in a slow-growing (light orange) and growth-arrested (dark orange) *lin-42(0)* animal, corresponding to the same individuals highlighted in (a). Markers indicate seam cell divisions (circles), wrt-2p::GFP peaks (squares) and ecdyses (triangles). The growth-arrested animal (dark orange) executed most events that occur after mid-L2, indicating the absence of a developmental arrest. **(d)** Developmental phase as function of time in wild-type (black) and *lin-42(0)* animals (orange). The phase evolution in *lin-*

42(0) animals was well fitted with the 'Rate change' model (orange line), with development occurring at approximately wild-type rate until the mid-L2 stage, and ~2-fold decreased rate for all events occurring later. **(e)** Measured times for event pairs: (1) division 1 and 3, (2) division 3 and peak 3, (3) peak 2 and ecdysis 3, and (4) division 4 and ecdysis 2. Lines are a fit to data for standard conditions. Overall, *lin-42(0)* animals show strong variability in timing between individuals, and for event pairs (2) and (3) exhibit clear deviations from scaling. **(f)** Deviation from scaling for development in *lin-42(0)* mutants. Stars indicate probability that *lin-42(0)* data observes the same scaling relation as wild-type: *:N.S., **:P<0.01, and P<0.001 otherwise (K-S test). Deviations from scaling resemble those predicted by the 'Rate change' model, with the dashed lines indicating the measured time of the rate change.

Restoration of population-level temporal scaling within developmental epochs

Both for wild-type animals fed *E. coli* HB101, and *lin-42(0)* mutants, we observed changes in timing of individual events compared to standard conditions that could not be explained by a simple rescaling with the population-averaged duration of development. In both cases, breakdown of scaling was linked to a discontinuity in the rate of development, either a pause (Fig. 4b) or change in rate of development (Fig. 5d), with deviations from scaling strongest for pairs of events on either side of the discontinuity. However, this raised the question, particularly for the timing mutant *lin-42*, whether the observed breakdown was explained fully by the discontinuity in developmental rate, or also reflected true misregulation of developmental timing. Our phenomenological models suggested a way to examine this further. Both in the 'Pause' and 'Rate change' model, the discontinuity divided development into two epochs of otherwise constant developmental rate (Fig. 6a). The model predicted that if we measured time not relative to hatching, but to an event occurring after the discontinuity, times of event pairs that both occurred after the discontinuity would fall along the same line as data for animals in standard conditions (Fig. 6b, Eq. 10), meaning that timing of events within a developmental epoch can be fully explained by rescaling with the population-averaged duration of that epoch.

We then tested this for the experimentally measured event times for wild-type animals on HB101 and *lin-42(0)* mutants, focusing on the events (*wrt-2* peak 2 – ecdysis 4) that occur after the discontinuity observed in the mid-L2 larval stage in both experiments. When we compared event pairs that showed deviations from scaling when time was measured relative to hatching, but now measured relative to time of the second *wrt-2* peak (Fig. 6d,f), we found that common variability, i.e. the spread of points along the scaling line, was reduced. Moreover, data points no

longer showed a systematic deviation from the scaling line, indicating that deviations from scaling were reduced. Indeed, when we compared deviations from scaling for all event pairs (Fig. 6e,g), we found that deviations from scaling were no longer significant for most event pairs, although some deviations remained, especially for *lin-42(0)* mutants. Overall, these results showed that despite a breakdown in temporal scaling with the population-averaged duration of development, event timing did exhibit temporal scaling within the duration of developmental epochs, even for *lin-42(0)* mutants, that showed a pronounced growth-arrest and strong variability in timing between individuals.

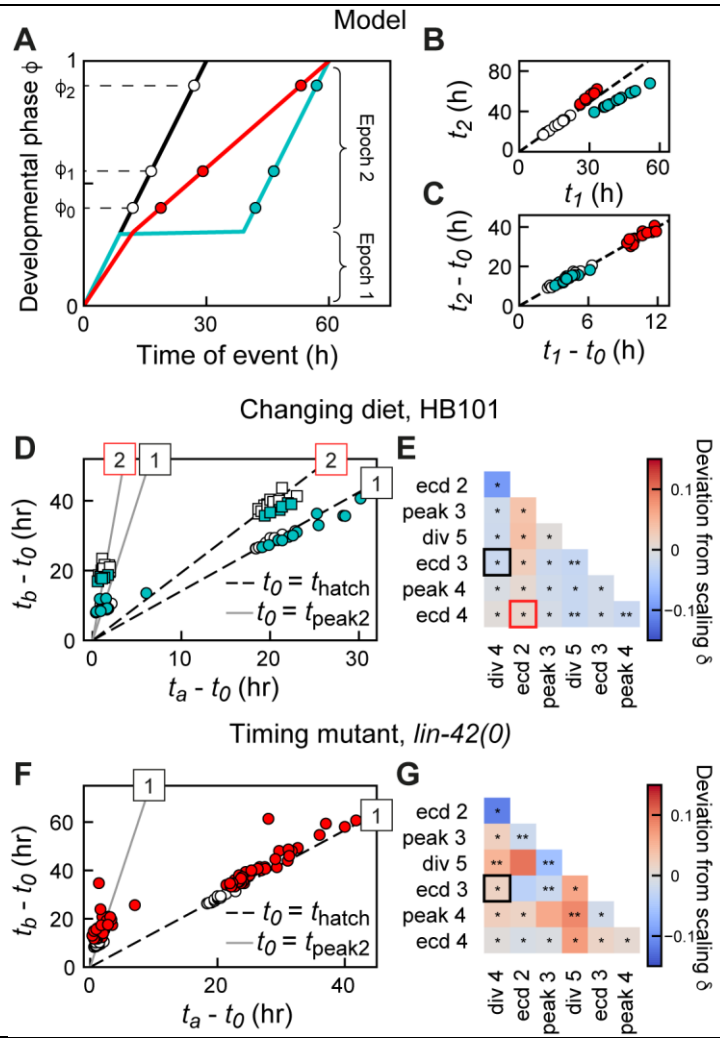

Figure 6. **Temporal scaling in epochs of constant developmental rate.**

(a)-(c) Both 'Pause' (blue) and 'Rate change' (red) timing models divide development in two epochs of constant developmental rate. The models predicted that, while timing of events pair *1* and *2* deviate from scaling when measured relative to the start of development (b), temporal scaling is observed when measured relative to an event *0* occurring within the same epoch (c).

Markers indicate simulated event pairs and dashed lines the scaling relationship for wild-type development. **(d),(e)** Measured times for event pairs in (d) wild-type animals fed on HB101 (blue markers) and (e) *lin-42(0)* mutants (red markers): (1) division 4 and ecdysis 3, and (2) ecdysis 2 and 4. Data is shown either relative to time of hatching or time of wrt-2p::GFP peak 2, the first event after the observed pause (HB101) and rate change (*lin-42*). White markers are wild-type data and dashed lines indicate wild-type scaling relationship. Deviations from scaling are reduced when measured relative to peak 2. **(f), (g)** Deviation from scaling for development on (f) HB101 diet and (g) in *lin-42(0)* mutants for all event pairs in the epoch following developmental pause (HB101) or rate change (*lin-42*). Stars give probability that HB101 or *lin-42(0)* data observes the same scaling relation as wild-type: *:N.S., **:P<0.01, and P<0.001 otherwise (K-S test). For most event pairs, deviations from scaling are not statistically significant.

Discussion

Here, we showed that changes in timing of individual developmental events, under a broad array of conditions that change the total duration of *C. elegans* larval development, are largely explained by temporal scaling, both for changes in timing due to variability between individuals and for population-level changes in timing resulting from shifts in environmental conditions or changes in genotype. To reach these conclusions, we studied qualitatively different events (seam cell division, cyclical *wrt-2* gene expression and ecdysis) that occur frequently during larval development, thereby maximizing the amount of timing data collected from measurements in single developing larvae. However, all these events take place in the same organ, the hypodermis, and are closely linked to the molting cycle, meaning that, potentially, they are not independent. It will be interesting to test whether the timing of pairs of events from different organs also follows temporal scaling relations, as expected when organs develop in synchrony, or whether relative timing between organs shifts under some conditions.

We found that many of our experimental observations could be reproduced by simple, phenomenological timing models (Fig. 3). In these models, the complexity of developmental progression is reduced to the evolution of a developmental phase in time, similar to the use of phase in the analysis of nonlinear oscillators. Animal-to-animal variability arises because each animal proceeds through its phase evolution at an intrinsically different rate, giving rise to the strongly correlated variability we measured for timing of event pairs. Changes in population-averaged timing, e.g. due to shifts in environmental conditions or differences in genotype, changed the evolution of phase in time, in a manner that specific to each environmental condition and genotype. These differences in the evolution of developmental phase were sufficient to explain the type and magnitude of deviations we observed experimentally in population-level scaling. While these models do not provide a mechanism for temporal scaling, they reveal a remarkably simple organization that unifies the striking variations in timing seen in our experiments.

It is a striking observation that isogenic animals under the same environmental conditions show considerable variability in total duration of development. This animal-to-animal variability has been observed before[18, 21], but here we characterized it systematically for multiple developmental events, and under different conditions. Interestingly, when comparing timing of event pairs, we found that this variability was highly correlated, with data for individual animals

clustered tightly along a line for most event pairs, a hallmark of scaling (Fig. 1e, 2c, 4c, 5e). This observation implies that individual animals proceed through development at a unique rate, that varies within the population but otherwise remains constant throughout larval development. It was found recently that individual variability in timing of the L4 ecdysis correlated with maternal age at time of fertilization, through age-dependent variation in the amount of vitellogens mothers loaded into their embryos[21]. Together with our results, this suggests that variability between embryos fully determines the systematic animal-to-animal variation in the rate of all subsequent larval development. However, in *lin-42(0)* animals, we found that this correlation in timing was absent for some event pairs (Fig. 5e). This observation challenges the idea that animal-to-animal variation in developmental are strictly set at the embryonic stage, and instead suggests that it might be impacted by conditions encountered during subsequent larval development.

For changes in conditions that exhibited population-level temporal scaling for all event pairs (changes in temperature, dietary restricted *eat-2* mutants), the rate of development was reduced by a constant factor (Figs. 2b, 4b). In contrast, both for wild-type animals fed HB101 and *lin-42(0)* mutants, we observed a discontinuity in the rate of development (Figs. 4b, 5d). Interestingly, even though the nature of the discontinuity differed, with a pause for animals fed HB101 and a change in rate for *lin-42(0)* mutants, in both cases it occurred at the same development stage: the mid-L2 larval stage between the third seam cell division and the second *wrt-2* peak. This developmental stage is notable, as it forms an important transition point both in terms of development and metabolism. First, under conditions of crowding or food deprivation larvae enter dauer, an alternative developmental state that is highly stress-resistant, and commit to this fate before the mid-L2 larval stage[34, 35]. Interestingly, *lin-42* is involved in dauer commitment, with *lin-42* mutants showing increased dauer formation at 27˚C[36]. Hence, change in rate of development at this stage might reflect involvement of the dauer decision-making machinery. However, we prefer another explanation: *C. elegans* larvae also shift their metabolism between the L1 and L2 larval stage, from the glyoxylate cycle to the TCA cycle[37]. The glyoxylate cycle likely allows L1 larvae to use stored lipids as an energy source, potentially rendering their development less dependent on ingestion of food. As a consequence, shifts in diet (from *E. coli* OP50 to HB1010) or inability to ingest or metabolize food in *lin-42(0)* mutants[27] might only impact developmental timing substantially after shifting to the TCA cycle. Overall, the fact that we observe temporal scaling for events that both occur before or after the mid-L2 stage (Fig. 6), even in *lin-42(0)* mutants where the rate of development exhibited an abrupt and substantial decrease, shows that the underlying timing mechanisms must be able to adjust themselves to such changes.

Our observations raise the question how temporal scaling is regulated. One attractive mechanism to regulate timing in a manner that is synchronized throughout the body and adapts to changes in rate of development under different conditions, is to couple developmental timing to physical growth. Analogously, cell cycle timing in unicellular organisms, such as bacteria or yeast, strongly depends on cell size and growth[38-41]. Indeed, progression of *C. elegans* larval development is tightly linked to body size[22], and under dietary conditions that caused slow growth, larval stages lengthened so that molts occurred at their stereotypical body size[4]. Moreover, conditions that do not allow growth, such as starvation, typically lead to developmental arrest at the start of each larval stage[42-44]. If timing was regulated in such a way that each event occurred at a specific body size, it would naturally explain temporal scaling, provided that changes in developmental rate under shifts in environmental conditions are accompanied by a concomitant change in the rate of body growth. It is therefore an important observation that *lin-42(0)* mutants continued development without physical growth (Fig. 4), and with timing of development explained by temporal scaling within epochs of constant developmental rate (Fig. 5). Continued development after growth arrest in *lin-42(0)* mutants was shown recently for motor neuron, gonad and vulva development[27], but timing was not examined. Our work now extends these observations, indicating that continued development without growth is likely a *lin-42(0)* phenotype with body-wide impact, and specifically invalidates a mechanism where temporal scaling results from coupling developmental timing to physical growth.

One of the most enduring mysteries of development is how its timing is regulated. Whereas we have a deep understanding of how spatial patterns arise during development, our understanding of how events like cell division, cell movement or gene expression are controlled in time is still very limited. Post-embryonic development poses a particular challenge, as its rate of progression depends strongly on environmental conditions such as food availability. How timing is adapted on the cellular level in response to such organism-level changes is an open question. On the molecular level, developmental timing is thought to be controlled either by oscillators or 'hourglass' mechanisms, where steady accumulation or degradation of proteins triggers events when a particular threshold is reached[45]. In *C. elegans*, even though there is now evidence both for hourglass mechanisms[46, 47] and oscillators[11, 14] in regulating timing of larval development, we still do not understand how the exact time at which cell-level events are initiated is determined on the molecular level. Both hour-glass and oscillator mechanisms cannot explain temporal scaling of developmental timing without substantial alterations to their core mechanism. Hence, our observation of temporal scaling will put strong constraints on

possible models that explain developmental timing of *C. elegans* larval development.

Materials and methods

Strains and experimental conditions

The following strains were used: SV1009 (*heIs63*[Pwrt-2::GFP::PH; Pwrt-2::GFP::H2B; Plin-48::mCherry], van den Heuvel lab)[14], DA1113 (*eat-2(ad1113)II*, CGC), RG1590 (*lin-42*(*ox461*), Rougvie lab)[18], RB1843 (*lin-42*(*ok2385*)*II*, CGC). To monitor *wrt-2::GFP* expression in *eat-2* and *lin-42* mutant animals, the corresponding strain was crossed with *heIs63*. The *eat-2* genotype was confirmed by measuring the rate of pharyngeal pumping, which is decreased 5-fold compared to wild-type animals[26]. As *lin-42* constitutes a complex genetic locus encoding multiple isoforms, we chose to use the *lin-42(ox461)* allele that deletes the entire locus of *lin-42[27].* In addition, the *lin-42(ok2385)* allele that deletes the main isoform *lin-42a* and the overlapping exons of *lin-42b*, was analyzed and showed similar phenotypes as *lin-42(ox461)* (data not shown).

For maintenance, all strains were cultured at 20˚C on NGM (Nematode growth medium) agar plates seeded with OP50 strain of *E. coli* bacteria, using standard *C. elegans* techniques. For time-lapse experiments, we refer to standard conditions as wrt2p::GFP animals fed on an *E. coli* OP50 diet at 23˚C. For experiments in perturbed conditions we varied one experimental parameter (*C. elegans* strain, temperature or diet) while keeping the others unchanged. For the diet experiment in Fig. 4, *E. coli* HB101 was used instead. In that case, animals were maintained on HB101 for 5-7 generations prior to the experiment.

Time-lapse microscopy

Custom time-lapse microscopy setup was used to monitor the entire development of individual *C. elegans*. Late-stage embryos were placed inside the 250x250x20 µm polyacrylamide microchambers (one embryo per chamber) filled with *E. coli* bacteria as food source. Nikon Ti-E inverted microscope with a large chip camera (Hamamatsu sCMOS Orca v2) and a 40x magnification objective (Nikon CFI Plan Fluor 40x, NA=1.3, oil immersion) were used for imaging. Transmission and fluorescence images were acquired with an LED light source (CoolLED pE-100 615nm) and a 488 nm laser (Coherent OBIS LS 488-100), respectively. Each chamber containing a single animal was imaged every 20-40 minutes during the entire larval

development (40-100 hours depending on the genotype and temperature). A stack of 20-30 images in the Z-direction was acquired using short exposure times (1-10 ms), such that the motion of the animal was insignificant. We have previously demonstrated that this technique does not hinder larval growth and development[18].

Temperature control

All experiments were performed in a temperature-controlled room with a constant temperature inside the sample of 23˚C. To perform an experiment at different temperature, an additional temperature control system was used. A thermoelectric chiller (Thermotek T257P) was used to cool the custom made objective jacket by circulating an antifreeze fluid (a mixture of water and glycerin) between the chiller and the objective jacket. In order to calibrate the system, a thermocouple temperature sensor measuring 0.025 mm in diameter (RS Pro) was placed inside the sample in contact with the polyacrylamide hydrogel and connected to a digital thermometer (RS Pro). The temperature was then varied on the thermoelectric chiller while the resulting temperature inside the sample was being monitored. In this work, experiments were performed at 23, 19 or 15 ˚C.

Image analysis

Time-lapse image stacks were processed with custom Python software in order to obtain the precise timing of ecdysis events, seam cell divisions, and peaks in oscillatory *wrt-2* expression. For every animal, the times of hatching and ecdysis events were annotated based on visual inspection of transmitted light images. Hatching was defined as the time larvae first appears out of the egg shell, while ecdysis events were defined as the first appearance of the shed cuticle in the chamber (Fig. 1c). Times of seam cell divisions were annotated based on visual inspection of *wrt-2*::GFP fluorescence in the nucleus and the membrane of seam cells. Divisions of V1-V6 seam cells occur close together in time and repeat 5 times during postembryonic development. We therefore defined the time of each round of divisions as the average time V1-V6 cells had divided or had started dividing, as determined by the formation of the metaphase plate. Due to light scattering through the worm's tissues, we could only analyze seam cells located on the body side closest to the objective.

To calculate times corresponding to peaks in oscillatory *wrt-2* expression, we first obtained *wrt-2* expression profiles as a function of time for individual animals. For this, in every time frame we automatically segmented the region encompassing seam cells using a Watershed algorithm and calculated the average fluorescence intensity inside this region. Finally, to find the time of each peak (μ_i), we fitted the obtained oscillatory profiles with a combination of Gaussian functions and a linear offset using non-linear least-squares minimization (Fig. 1b):

$$f(x, m, b, A_i, \mu_i, \sigma_i) = mx + b + \sum_{i=1}^{n} \left[\frac{A_i}{\sigma_i \sqrt{2\pi}} e^{\left[-\frac{(x-\mu_i)^2}{2\sigma_i^2}\right]} \right] \quad (1)$$

where *n* is the number of peaks, A_i, μ_i, σ_i are the amplitude, center and width of peak. Finally, we fitted the experimentally measured times for pairs of events a and b to a line function of the form $t_b = s_{a,b} \cdot t_a$ using non-linear least-squares minimization (Fig. 1e), using the Linear Model from the *lmfit* package in Python. To measure the animal's body length as a function of time (Fig. 5a), we manually annotated ~10 points along the anterior-posterior body axis and performed spline interpolation. Body length was defined as the length of the resulting spline curve.

Stochastic timing model and simulations

We model the progression of development as the evolution of a developmental phase ϕ, that increases from ϕ=0 (start of larval development at hatching) to ϕ=1 (entry into adulthood at the L4 molt). The exact assignment of a phase to a particular developmental event is arbitrary. Here, we define the phase so that for standard conditions (wild-type animals at 23 ˚C) the phase increases linearly with time, $\frac{d\phi}{dt}$=const, and ϕ=1 at time t=T, where T is the total duration of development at standard conditions. As a result, for standard conditions we the following definition for the developmental phase of event a:

$$\phi_a = \frac{t_a}{T} \quad (2)$$

For other conditions or genotypes, the time evolution $\phi(t)$ of the developmental phase has a different form. As a result, the time of event a, occurring at a developmental phase ϕ_a is given by $t_a = f(\phi_a)$, where f is a monotonically increasing function that is specific for each condition or genotype. Expressions for $f(\phi)$ are discussed further below.

To incorporate animal-to-animal variability, we assumed two different sources of variability. First, there is an intrinsic variability in the stage ϕ_a at which each event a occurs, that is uncorrelated between different events occurring within the same animal. Second, we assumed variability in the total duration of development, T. This corresponds to an animal-to-animal variability in the global rate of development that impacts each event occurring within the same animal equally. Then, the event time $t_{a,i}$ for event a in animal i is given by:

$$t_{a,i} = \frac{f\left(\phi_a + \eta_{\phi,i}\right)}{T}(T + \eta_{T,i}) \tag{3}$$

where, T and ϕ_a correspond to the population average values, while η_T and η_ϕ are Gaussian noise sources with standard deviation σ_T and σ_ϕ, respectively.

The function $f(\phi)$ changes for differing environmental conditions or mutants that perturb the duration of development. In particular, we considered three different models, the 'Uniform', 'Pause', and 'Rate change' models (Fig. 3a). For the 'Uniform' model, event times are given by Eq. 2, but now with an increased duration for development T'. For the 'Pause' model, developmental occurs at the same rate as for standard conditions, but with a pause at developmental phase ϕ' that results in a total duration of development $T' = (1 + \kappa)T$, resulting in:

$$t_a = \begin{cases} T\phi_a & \phi_a < \phi' \\ T(\kappa + \phi_a) & \phi_a \geq \phi' \end{cases} \tag{4}$$

Finally, for the 'Rate change' the developmental rate differs between events occurring prior to a developmental phase ϕ'' and events occurring afterwards, resulting in:

$$t_a = \begin{cases} T_1\phi_a & \phi_a < \phi'' \\ (T_1 - T_2)\phi'' + T_2\phi_a & \phi_a \geq \phi'' \end{cases} \tag{5}$$

where $1/T_1$ and $1/T_2$ correspond to the two developmental rates and the total duration of development is given by $T' = T_1\phi'' + T_2(1 - \phi'')$.

Calculation of deviation from scaling for timing models

For the 'Uniform', 'Pause' and 'Rate change' model, we calculate the deviation from scaling as follows. First, we use that fact that for events a and b that occur in the same animal, the total

duration of development, T', has the same value, to express t_b as function of t_a. For the 'Uniform' model, this yields:

$$t_b = \frac{\phi_b}{\phi_a} t_a \tag{6}$$

meaning that that event pairs lie along the same line as measured for individuals under standard conditions, and that the changes in timing can be fully captured by a simple rescaling of event times with the duration of development T' under non-standard conditions. In contrast, for the 'Pause' model, this yields:

$$t_b = \begin{cases} \frac{\phi_b}{\phi_a} t_a & t_a, t_b < t^* \\ \frac{\kappa + \phi_b}{\phi_a} t_a & t_a < t^*, t_b > t^* \\ \frac{\kappa + \phi_b}{\kappa + \phi_a} t_a & t_a, t_b > t^* \end{cases} \tag{7}$$

Here, pairs of time points for events a and b only lie along the same line as those for standard conditions when both events occur before the time of the delay, $t^* = T\phi'$. Otherwise, the slope of the line is different from wild-type conditions and depends explicitly on the delay parameter κ. Finally, for 'Rate change' model, corresponding to the *lin-42(ox461)* mutant, we have:

$$t_b = \begin{cases} \frac{\phi_b}{\phi_a} t_a & t_a, t_b < t^* \\ \left(\frac{\phi''}{\phi_a} + \frac{T_2}{T_1} \frac{\phi_b - \phi''}{\phi_a} \right) t_a & t_a < t^*, t_b > t^* \\ \frac{T_1 \phi'' + T_2 (\phi_b - \phi'')}{T_1 \phi'' + T_2 (\phi_a - \phi'')} t_a & t_a, t_b > t^* \end{cases} \tag{8}$$

where $t^* = T_1 \phi''$. Apart from the case when $t_a, t_b < t^*$, this expression depends explicitly on the parameters ϕ'' and T_2 and does not lie along the same line event pairs for standard conditions. Finally, we calculate the deviation from scaling as:

$$\delta_{ab} = \mathrm{atan}(s_{ab}^S) - \mathrm{atan}\,(s_{ab}^P) \tag{9}$$

where $t_b = s_{ab} \cdot t_a$ and S and P denotes the slope for standard and perturbed conditions, respectively.

Temporal scaling in epochs of constant developmental rate

If we compare the timing of two events a and b relative to the time of a third event c, e.g. the L2 *wrt-2* peak as in Fig. 6d-g, such that $t_a, t_b, t_c > t^*$, then we find that for all models:

$$(t_b\text{-}t_c) = \frac{\phi_b\text{-}\phi_c}{\phi_a\text{-}\phi_c}(t_a\text{-}t_c) \tag{10}$$

independent of any other model parameters, as long as all three events a,b,c occur in an epoch of constant developmental rate. This means that when considering events that occur after the discontinuity in developmental rate at time t^*, as seen in the 'Pause' and 'Rate change' Model, their timing relative to event c still shows temporal scaling, meaning that all events occur at the same time relative to the duration of that developmental epoch, e.g. L2 to L4 ecdysis as in Fig. 6.

Calculating the deviation from scaling for experimental data

We used the following procedure to assess whether the timing of event pairs a and b under perturbed conditions P deviate from the scaling relationship found for their timing under standard conditions S. For each animal i with measured event timing $t_{a,i}$ and $t_{b,i}$, we calculate $\theta_i = \arctan\frac{t_{a,i}-t_{0,i}}{t_{b,i}-t_{0,i}}$. Here, $t_{0,i}$ is the time of an event relative to which the timing of the event pair is assessed. Unless mentioned otherwise, this is the time of hatching, i.e. $t_{0,i}=0$. First, we calculate the average deviation δ from scaling as $\delta=\langle\theta_i^P\rangle\text{-}\langle\theta_i^S\rangle$. However, in particular for event pairs with small average event times $\langle t_{a,i}\text{-}t_{0,i}\rangle$ and $\langle t_{b,i}\text{-}t_{0,i}\rangle$, values of θ_i can vary substantially, leading to non-zero deviation δ for the typical number of animals analyzed for these experiments. Hence, we also estimate the probability that the two series θ_i^P and θ_i^S are sampled from the same distribution, using the two-sample Kolmogorov-Smirnov test (*ks_2samp* from the *scipy.stats* package in Python). We reported the P value, with high P meaning that the distributions of the two samples are likely the same.

References

1. Ebisuya, M. and J. Briscoe, *What does time mean in development?* 2018. **145**(12).
2. Moss, E.G., *Heterochronic genes and the nature of developmental time.* Curr Biol, 2007. **17**(11): p. R425-34.
3. Rougvie, A.E., *Control of developmental timing in animals.* Development, 2001. **2**(9): p. 690-701.
4. Uppaluri, S. and C.P. Brangwynne, *A size threshold governs Caenorhabditis elegans developmental progression.* Proceedings of the Royal Society B: Biological Sciences, 2015. **282**(1813): p. 20151283.
5. Ben-Zvi, D., et al., *Scaling of the BMP activation gradient in Xenopus embryos.* Nature, 2008. **453**(7199): p. 1205-11.
6. Gregor, T., et al., *Diffusion and scaling during early embryonic pattern formation.* Proc Natl Acad Sci U S A, 2005. **102**(51): p. 18403-7.
7. Houchmandzadeh, B., E. Wieschaus, and S. Leibler, *Establishment of developmental precision and proportions in the early Drosophila embryo.* Nature, 2002. **415**(6873): p. 798-802.
8. Umulis, D.M. and H.G. Othmer, *Mechanisms of scaling in pattern formation.* Development, 2013. **140**(24): p. 4830-43.
9. Driever, W. and C. Nüsslein-Volhard, *A gradient of bicoid protein in Drosophila embryos.* Cell, 1988. **54**(1): p. 83-93.
10. Driever, W. and C. Nüsslein-Volhard, *The bicoid protein determines position in the Drosophila embryo in a concentration-dependent manner.* Cell, 1988. **54**(1): p. 95-104.
11. Monsalve, G.C. and A.R. Frand, *Toward a unified model of developmental timing: A "molting" approach.* Worm, 2012. **1**(4): p. 221-30.
12. Hendriks, G.J., et al., *Extensive oscillatory gene expression during C. elegans larval development.* Mol Syst Biol, 2014. **53**(3): p. 380-92.
13. Kim, D., D. Grün, and A. van Oudenaarden, *Dampening of expression oscillations by synchronous regulation of a microRNA and its target.* Mol Cell, 2013. **45**(11): p. 1337-44.
14. Meeuse, M.W. and Y.P. Hauser, *Developmental function and state transitions of a gene expression oscillator in Caenorhabditis elegans.* 2020. **16**(7): p. e9498.
15. Ambros, V. and H.R. Horvitz, *Heterochronic mutants of the nematode Caenorhabditis elegans.* Science, 1984. **226**(4673): p. 409-16.

16. Monsalve, G.C., C. Van Buskirk, and A.R. Frand, *LIN-42/PERIOD controls cyclical and developmental progression of C. elegans molts.* Curr Biol, 2011. **21**(24): p. 2033-45.
17. Jeon, M., et al., *Similarity of the C. elegans developmental timing protein LIN-42 to circadian rhythm proteins.* Science, 1999. **286**(5442): p. 1141-6.
18. Gritti, N., et al., *Long-term time-lapse microscopy of C. elegans post-embryonic development.* Nat Commun, 2016. **7**: p. 12500.
19. Sulston, J.E. and H.R. Horvitz, *Post-embryonic cell lineages of the nematode, Caenorhabditis elegans.* Dev Biol, 1977. **56**(1): p. 110-56.
20. Wildwater, M., et al., *Cell shape and Wnt signaling redundantly control the division axis of C. elegans epithelial stem cells.* Development, 2011. **138**(20): p. 4375-85.
21. Perez, M.F., et al., *Maternal age generates phenotypic variation in Caenorhabditis elegans.* Nature, 2017. **552**(7683): p. 106-109.
22. Byerly, L., R.C. Cassada, and R.L. Russell, *The life cycle of the nematode Caenorhabditis elegans. I. Wild-type growth and reproduction.* Dev Biol, 1976. **51**(1): p. 23-33.
23. Avery, L. and B.B. Shtonda, *Food transport in the C. elegans pharynx.* J Exp Biol, 2003. **206**(Pt 14): p. 2441-57.
24. MacNeil, L.T., et al., *Diet-induced developmental acceleration independent of TOR and insulin in C. elegans.* Cell, 2013. **153**(1): p. 240-52.
25. Soukas, A.A., et al., *Rictor/TORC2 regulates fat metabolism, feeding, growth, and life span in Caenorhabditis elegans.* Genes Dev, 2009. **23**(4): p. 496-511.
26. Raizen, D.M., R.Y. Lee, and L. Avery, *Interacting genes required for pharyngeal excitation by motor neuron MC in Caenorhabditis elegans.* Genetics, 1995. **141**(4): p. 1365-82.
27. Edelman, T.L., et al., *Analysis of a lin-42/period Null Allele Implicates All Three Isoforms in Regulation of Caenorhabditis elegans Molting and Developmental Timing.* G3 (Bethesda), 2016. **6**(12): p. 4077-4086.
28. Olmedo, M., et al., *A high-throughput method for the analysis of larval developmental phenotypes in Caenorhabditis elegans.* Genetics, 2015. **201**(2): p. 443-448.
29. Abrahante, J.E., E.A. Miller, and A.E. Rougvie, *Identification of heterochronic mutants in Caenorhabditis elegans. Temporal misexpression of a collagen::green fluorescent protein fusion gene.* Genetics, 1998. **149**(3): p. 1335-51.
30. Tennessen, J.M., et al., *Novel heterochronic functions of the Caenorhabditis elegans period-related protein LIN-42.* Dev Biol, 2006. **289**(1): p. 30-43.

31. McCulloch, K.A. and A.E. Rougvie, *Caenorhabditis elegans period homolog lin-42 regulates the timing of heterochronic miRNA expression.* Proc Natl Acad Sci U S A, 2014. **111**(43): p. 15450-5.
32. Perales, R., et al., *LIN-42, the Caenorhabditis elegans PERIOD homolog, negatively regulates microRNA transcription.* PLoS Genet, 2014. **10**(7): p. e1004486.
33. Van Wynsberghe, P.M. and A.E. Pasquinelli, *Period homolog LIN-42 regulates miRNA transcription to impact developmental timing.* Worm, 2014. **3**(4): p. e974453.
34. Golden, J.W. and D.L. Riddle, *The Caenorhabditis elegans dauer larva: developmental effects of pheromone, food, and temperature.* Dev Biol, 1984. **102**(2): p. 368-78.
35. Schaedel, O.N., et al., *Hormonal signal amplification mediates environmental conditions during development and controls an irreversible commitment to adulthood.* PLoS Biol, 2012. **10**(4): p. e1001306.
36. Tennessen, J.M., K.J. Opperman, and A.E. Rougvie, *The C. elegans developmental timing protein LIN-42 regulates diapause in response to environmental cues.* Development, 2010. **137**(20): p. 3501-11.
37. Wadsworth, W.G. and D.L. Riddle, *Developmental regulation of energy metabolism in Caenorhabditis elegans.* Dev Biol, 1989. **132**(1): p. 167-73.
38. Cooper, S. and C.E. Helmstetter, *Chromosome replication and the division cycle of Escherichia coli B/r.* J Mol Biol, 1968. **31**(3): p. 519-40.
39. Johnston, G.C., J.R. Pringle, and L.H. Hartwell, *Coordination of growth with cell division in the yeast Saccharomyces cerevisiae.* Exp Cell Res, 1977. **105**(1): p. 79-98.
40. Mitchison, J.M. and J. Creanor, *Further measurements of DNA synthesis and enzyme potential during cell cycle of fission yeast Schizosaccharomyces pombe.* Exp Cell Res, 1971. **69**(1): p. 244-7.
41. Robert, L., *Size sensors in bacteria, cell cycle control, and size control.* Front Microbiol, 2015. **6**: p. 515.
42. Baugh, L.R., *To grow or not to grow: nutritional control of development during Caenorhabditis elegans L1 arrest.* Genetics, 2013. **194**(3): p. 539-55.
43. Hu, P.J., *Dauer.* WormBook, 2007: p. 1-19.
44. Schindler, A.J., L.R. Baugh, and D.R. Sherwood, *Identification of late larval stage developmental checkpoints in Caenorhabditis elegans regulated by insulin/IGF and steroid hormone signaling pathways.* PLoS Genet, 2014. **10**(6): p. e1004426.
45. Rensing, L., U. Meyer-Grahle, and P. Ruoff, *Biological timing and the clock metaphor: oscillatory and hourglass mechanisms.* Chronobiol Int, 2001. **18**(3): p. 329-69.

46. Moss, E.G., R.C. Lee, and V. Ambros, *The cold shock domain protein LIN-28 controls developmental timing in C. elegans and is regulated by the lin-4 RNA.* Cell, 1997. **88**(5): p. 637-46.

47. Ruvkun, G. and J. Giusto, *The Caenorhabditis elegans heterochronic gene lin-14 encodes a nuclear protein that forms a temporal developmental switch.* Nature, 1989. **338**(6213): p. 313-9.

Supplementary figures

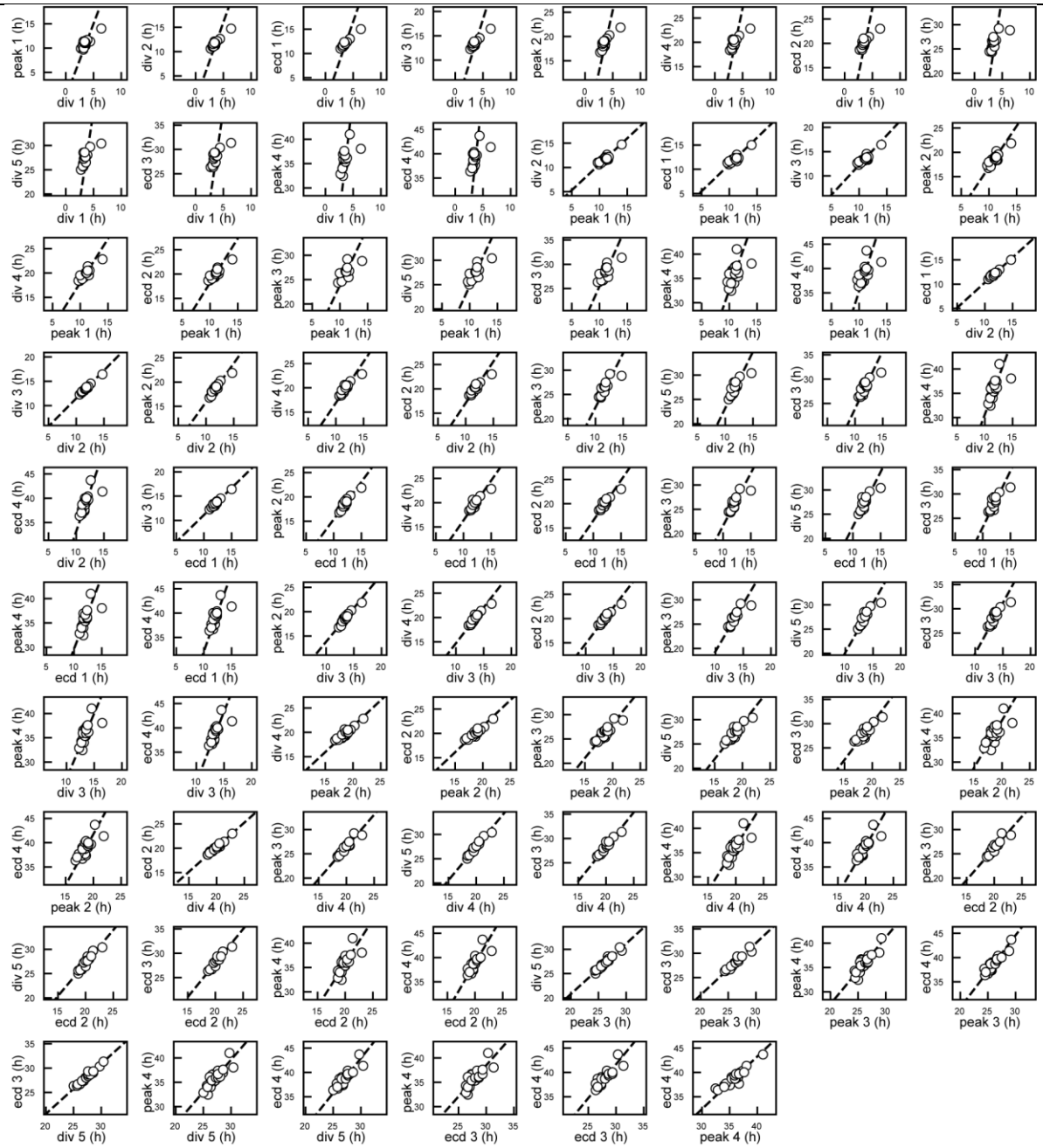

Supplementary Fig. 1. **Temporal scaling in animal-to-animal variability of timing.**

Measured times of for all measured event pairs a, b in wild-type animals, on an *E. coli* OP50 diet at 23˚C. Markers correspond to times measured in a single animal. Dashed lines are fits of the form $t_b = s_{a,b} \cdot t_a$.

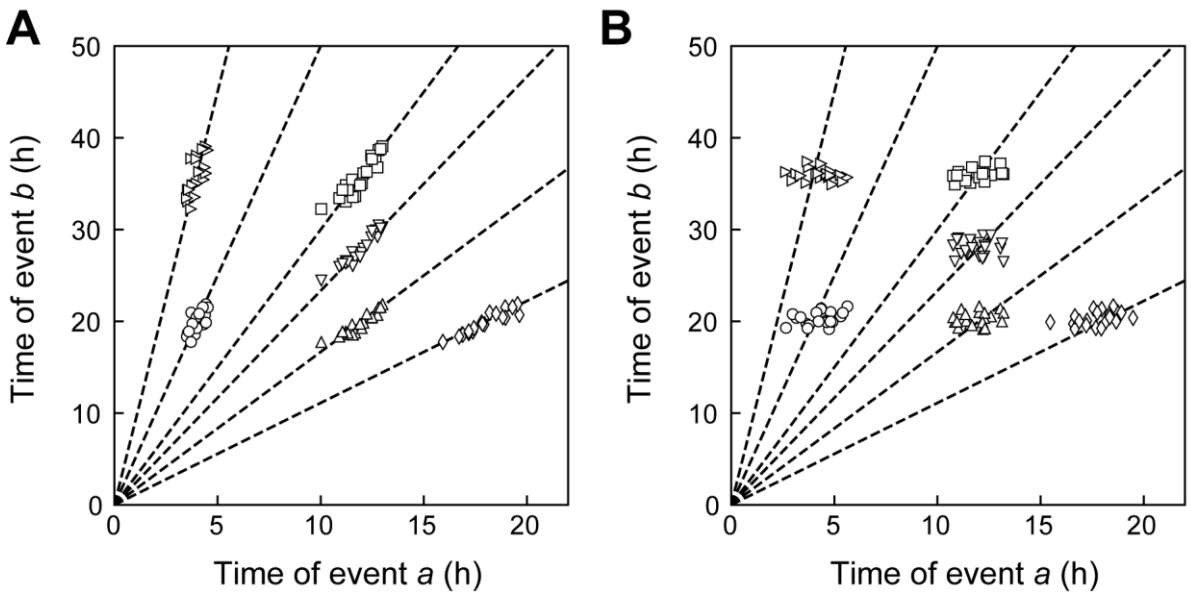

Supplementary Fig. 2. **Stochastic timing model**

(A) Simulated times of event pairs a, b in the stochastic timing model (Eqs. 2 and 3 in Methods). Simulation parameters were chosen to resemble the experimental data in Fig. 1e. Times were generated for six event, a-f, that occur at developmental phases The average duration of development was T=40h. For the noise sources, we used standard deviations σ_T=$3h$ and σ_ϕ=$7{\cdot}10^{-3}$, meaning that common variability in the rate of development, $1/T$, is stronger than variability in timing of each individual event. The simulated data closely resembles the experimental data in Fig. 1e, with times for event pairs a, b scattered along lines of $t_b = \frac{\phi_b}{\phi_a}\, t_a$ (dashed lines). **(B)** Same simulation as in (A), but now with standard deviations σ_T=$0.1h$ and σ_ϕ=$2{\cdot}10^{-2}$, meaning that variability in the timing of individual events is stronger than that in the global rate of development. As a consequence, times for event pairs no longer cluster along lines of $t_b = \frac{\phi_b}{\phi_a}\, t_a$ (dashed lines).

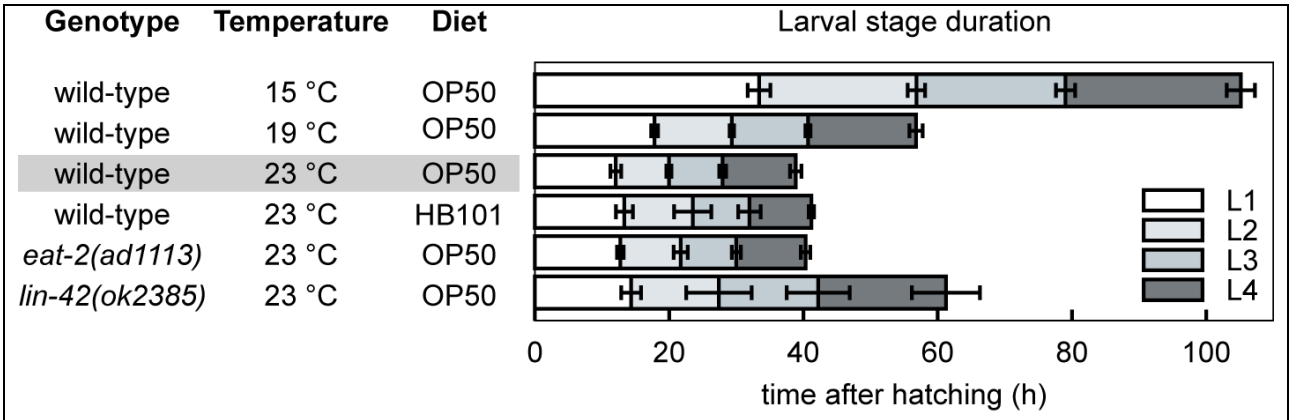

Supplementary Figure 3. **Overview of genotypes and conditions**.

Average duration of larval stages L1-L4 for the different genotypes and environmental conditions used. Wild-type refers to animals carrying only the *wrt-2p::GFP* reporter, which exhibit timing of larval stages similar to animals without this reporter. Strains with genotype different than wild-type also carry the *wrt-2p::GFP* reporter. OP50 and HB101 refer to different *E. coli* bacterial strains used a food source. The standard condition used as benchmark to compare event timing against is outlined in grey. For larval stage duration error bars indicate SD and for each condition n>7, except for lin-42 mutants, where only a few animals complete the L4 stage (n=4).

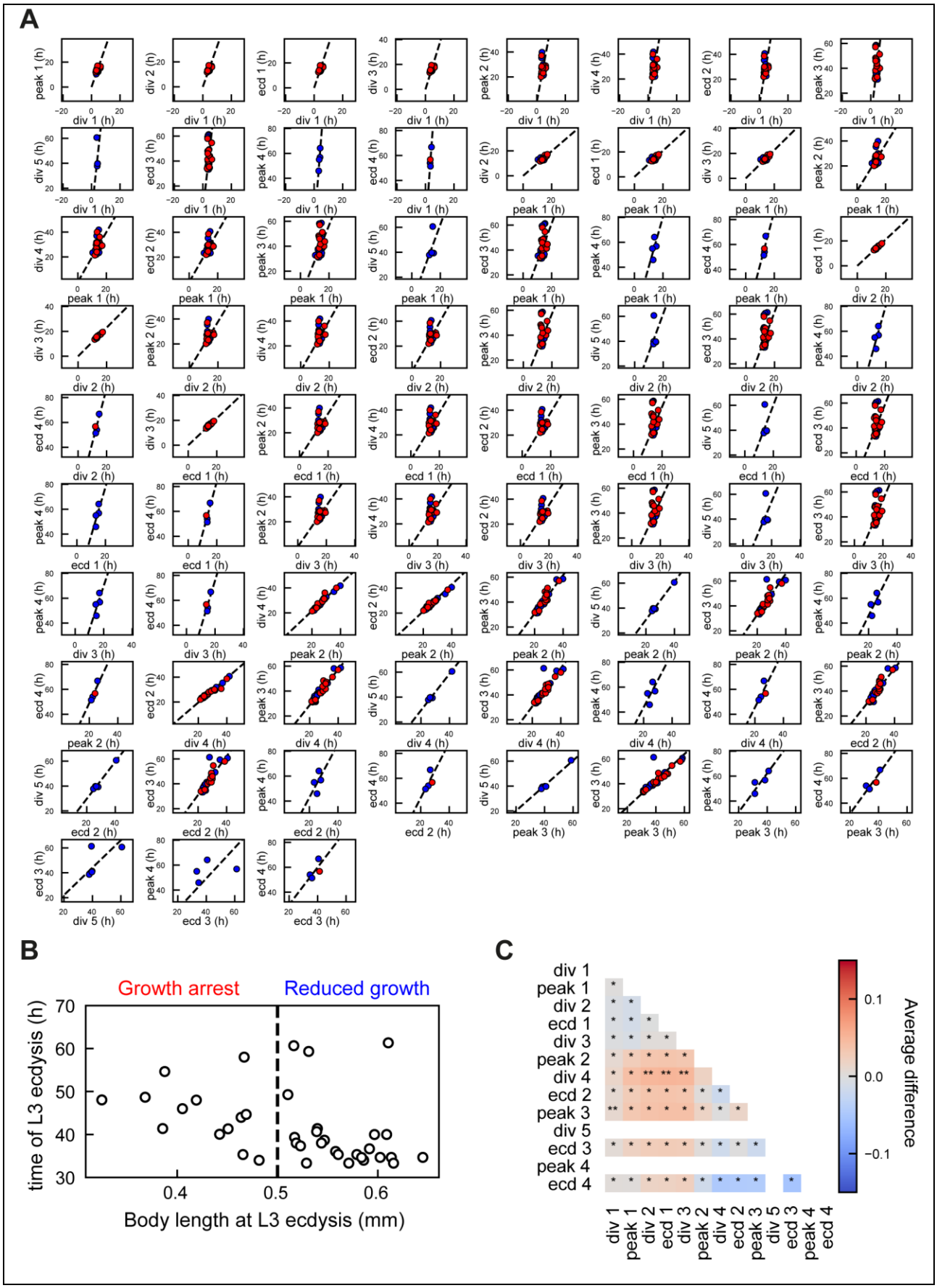
A
B
Growth arrest
Reduced growth
time of L3 ecdysis (h)
Body length at L3 ecdysis (mm)
C
Average difference
div 1
peak 1
div 2
ecd 1
div 3
peak 2
div 4
ecd 2
peak 3
div 5
ecd 3
peak 4
ecd 4

Supplementary Figure 4. **Dependence of deviation from temporal scaling on *lin-42(0)* growth arrest phenotype.**

(A) Measured times for all event pairs measured for at least $n \geq 4$ animals. Some event pairs found during wild-type L4 larval stage development do not appear as they are executed only rarely in *lin-42(0)* animals. Lines are a linear fit to the data points. Markers are colored according to growth phenotype, as defined in panel (b). The degree of deviation from scaling does not differ strongly between growth-arrested animals (red) and animals with reduced growth (blue). **(B)** Length at L3 ecdysis compared to time of L3 ecdysis in *lin-42(0)* animals. Based on this, we separated the population in growth-arrested animals (length < 0.5mm at L3 ecdysis) and animals with reduced growth, compared to wild-type animals. Growth-arrested animals developed more slowly than animals with reduced growth, but a small number of animals with reduced growth also displayed very slow development (L3 ecdysis later than 50 h after hatching). We scored the growth phenotype based on L3 characteristics, because most animals skip the L4 larval stage. **(C)** Difference in scaling between growth-arrested (GA) and reduce-growth (RG) animals. Color indicates the difference $\langle \theta^{GA} \rangle - \langle \theta^{RG} \rangle$ between the two populations, where, for each event pair a and b measured in an individual animal, the angle $\theta = \arctan \frac{t_a}{t_b}$. Stars indicate the probability that the distribution of θ is the same for growth-arrested and reduced-growth animals: *:N.S., **:P<0.01, and P<0.001 otherwise (K-S test). Overall, no significant differences in scaling were observed between growth-arrested and reduced-growth animals, indicating that growth-arrested animals do not display stronger breakdown of scaling. Empty squares reflect event pairs for which at least one of the two events did not occur in either growth-arrested or reduced-growth animals.